Temperature-driven 5f itinerant–localized crossover in the heavy-fermion compound $PuIn_3$

Haiyan Lu* and Li Huang
Science and Technology on Surface Physics and Chemistry Laboratory, P.O. Box 9-35, Jiangyou 621908, China

(Received 11 February 2021; revised 10 April 2021; accepted 6 May 2021; published 18 May 2021)

The temperature-dependent evolution pattern of 5f electrons helps to elucidate the long-standing itinerant-localized dual nature in plutonium-based compounds. In this work, we investigate the correlated electronic states of $PuIn_3$ dependence on temperature by using a combination of the density functional theory and the dynamical mean-field theory. Not only is the experimental photoemission spectroscopy reproduced, but also a 5f itinerant-localized crossover is identified. Moreover, it is found that the quasiparticle multiplets from the many-body transitions gradually enhance with decreasing temperature, accompanied by the hybridizations with 5f electrons and conduction bands. The temperature-induced variation of Fermi surface topology suggests a possible electronic Lifshitz transition and the onset of magnetic order at low temperature. Finally, the ubiquitous existence orbital selective 5f electronic correlation is also discovered in $PuIn_3$. These illuminating results shall enrich the understanding on Pu-based compounds and serve as critical predictions for ongoing experimental research.

DOI: 10.1103/PhysRevB.103.205134

I. INTRODUCTION

Plutonium (Pu) situates on the edge between the obviously hybridized 5f states of uranium [1] and mostly localized 5f states of americium [2], signifying the itinerant-localized nature of 5f electrons [3,4]. The spatial extension of partially filled 5f states enables the hybridization with conduction bands, facilitating active chemical bonding and formation of abundant plutonium-based compounds. In addition to the fantastic physical properties of Pu which are governed by the 5f states [5–11], the Pu-based compounds demonstrate novel quantum phenomena including unconventional superconductivity [12–16], nontrivial topology [17,18], complicated magnetic order [19], and heavy-fermion behavior [20], to name a few. The discovery of superconductivity in $PuCoGa_5$ [13–16] with an astonishingly high transition temperature of 18.5 K has renewed an interest in Pu-based compounds. The unconventional superconductivity in Pu-based "115" system ($PuMX_5$, M = Co, Rh; X = Ga, In) is intimately intertwined with 5f electrons which manifest themselves in plenty of ground-state properties comprising magnetism, superconductivity, and charge density wave [21,22].

$PuIn_3$ crystallizes in cubic $AuCu_3$ structure (space group Pm-3m) [see Fig. 1(a)] with lattice constant 4.703 Å [23], which is the parent material of $PuCoIn_5$ with the insertion of the $CoIn_2$ layer into the cubic structure. $PuIn_3$ is a paradigm Pu-based heavy-fermion compound [20] with an electronic specific heat coefficient of 307 mJ/(mol × K^2), suggesting a substantial effective mass enhancement. Moreover, the measured temperature dependence of electrical resistivity decreases rapidly below 50 K, displaying representative heavy-fermion behavior. Since the Pu-Pu distance in $PuIn_3$ is larger than the Hill limit, the specific heat, electrical resistivity, magnetic susceptibility, and ^{115}In nuclear quadrupole resonance [19] experiments all indicate the onset of antiferromagnetic order (AFM) below T_N = 14.5 K. So far, the commensurate AFM and its underlying mechanism is controversial and deserves further clarification [19,24]. Meanwhile, the de Haas–van Alphen (dHvA) oscillation identifies a Fermi surface pocket near the [111] direction with an enhanced cyclotron effective mass both in paramagnetic phase [25,26] and antiferromagnetic state [27]. The impact of magnetism on the heavy-fermion state with effective mass renormalization is another interesting issue. It is notable that the heavy-fermion state and antiferromagnetic order are closely related to the intricate electronic structure of $PuIn_3$. The experimental photoemission spectroscopy of $PuIn_3$ above T_N shows one peak around the Fermi level and the main peak at −1.2 eV, combined with mixed level model calculation within density functional theory (DFT), implying the itinerant-localized dual nature of 5f electrons [28]. On the theoretical side, the electronic structure, three-dimensional Fermi surface, dHvA quantum oscillation frequency and effective band mass in both the paramagnetic and antiferromagnetic states of $PuIn_3$ have been systematically addressed based on the density functional theory with a generalized gradient approximation [24]. Even though great efforts have been made to gain valuable insight into the itinerant-localized nature of 5f states. Only one of the three calculated Fermi surfaces on the basis of the 5f-itinerant band model [25] has been observed by the dHvA experiment. In addition, the experimental photoemission spectroscopy is well reproduced by employing the mixed level model [28] seems not quite consistent with the subsequent calculations [24]. The inconsistency might come from different approximations in traditional first-principles approaches. The itinerant degree of 5f states is not quantitatively described

*hyluphys@163.com

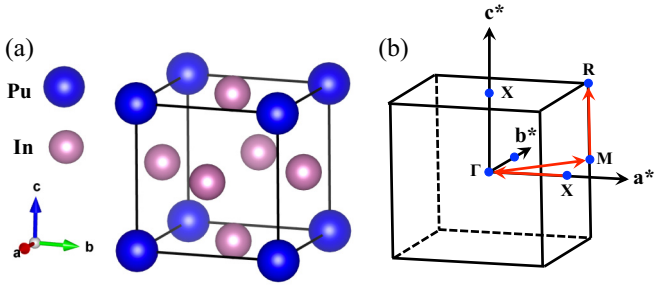

FIG. 1. (a) Crystal structure of $PuIn_3$. (b) Schematic picture of the first Brillouin zone of $PuIn_3$. Some high-symmetry k points X [0.5, 0.0, 0.0], Γ [0.0, 0.0, 0.0], M [0.5, 0.5, 0.0], and R [0.5, 0.5, 0.5] are marked.

without rigorous treating many-body effects. In addition, the ground-state calculation fails to access the finite-temperature effects. It is instructive to study the evolution of electronic structure as a function of temperature to probe the low-temperature magnetic state. Furthermore, large spin-orbital coupling and complicated magnetic ordering states make the theoretical calculations rather difficult. Accordingly, it seems tough to acquire an accurate and comprehensive picture for the electronic structure of $PuIn_3$.

In the paper, we present the electronic structure of $PuIn_3$ dependence on temperature using the density functional theory in combination with the single-site dynamical mean-field theory (DFT + DMFT). A comparative study of $PuIn_3$ shall shed light on the bonding behavior and correlation effects, so as to develop a deeper understanding of the relationships between electronic structure and antiferromagnetic state. We endeavor to elucidate the itinerant-localized $5f$ states. We calculate the momentum-resolved spectral functions, density of states, Fermi surface, self-energy functions, and valence state fluctuations of $PuIn_3$. It is discovered that $5f$ states become itinerant at low-temperature accompanied by moderate valence-state fluctuations. Moreover, the change of Fermi surface topology possibly implies the development of antiferromagnetic order. Finally, it is found that strongly correlated $5f$ electrons are orbital dependent, which seems to commonly exist in Pu-based compounds.

The rest of this paper is organized as follows. In Sec. II, the computational details are introduced. In Sec. III, the electronic band structures, total, and partial $5f$ density of states, Fermi surface topology, $5f$ self-energy functions, and probabilities of atomic eigenstates are presented. In Sec. IV, we attempt to clarify the $4f$ and $5f$ electrons in isostructural compounds $CeIn_3$ and $PuIn_3$. Finally, Sec. V serves as a brief conclusion.

II. METHODS

The well-established DFT + DMFT method combines realistic band-structure calculation by DFT with the nonperturbative many-body treatment of local interaction effects in DMFT [29,30]. Here we perform charge fully self-consistent calculations to explore the detailed electronic structure of $PuIn_3$ using the DFT + DMFT method. The implementation of this method is divided into DFT and DMFT parts, which are solved separately by using the WIEN2K code [31] and the EDMFTF package [32].

In the DFT calculation, the experimental crystal structure of $PuIn_3$ [23] was used. Since the calculated temperature is above the antiferromagnetic transition temperature, the system was assumed to be nonmagnetic. The generalized gradient approximation was adopted to formulate the exchange-correlation functional [33]. The spin-orbit coupling was taken into account in a second-order variational manner. The k-points' mesh was $15 \times 15 \times 15$ and $R_{\mathrm{MT}}K_{\mathrm{MAX}} = 8.0$.

In the DMFT part, $5f$ orbitals of plutonium were treated as correlated. The four-fermions' interaction matrix was parameterized using the Coulomb interaction $U = 5.0$ eV and the Hund's exchange $J_H = 0.6$ eV via the Slater integrals [34]. The fully localized limit scheme was used to calculate the double-counting term for impurity self-energy function [35]. The vertex-corrected one-crossing approximation (OCA) impurity solver [36] was employed to solve the resulting multiorbital Anderson impurity models. Note that we not only utilized the good quantum numbers N (total occupancy) and J (total angular momentum) to classify the atomic eigenstates, but also made a severe truncation ($N \in [3, 7]$) for the local Hilbert space [37] to reduce the computational burden. The convergence criteria for charge and energy were 10^{-5} e and 10^{-5} Ry, respectively. It is worth mentioning that the advantage of OCA impurity solver lies in the real axis self-energy, the direct output $\Sigma(\omega)$ was applied to calculate the momentum-resolved spectral functions $A(\mathbf{k}, \omega)$ and density of states $A(\omega)$, as well as other physical observables.

III. RESULTS OF $PuIn_3$

A. Momentum-resolved spectral functions

To ascertain the reliability of our calculations, we evaluate the momentum-resolved spectral functions $A(\mathbf{k}, \omega)$ of $PuIn_3$ along the high-symmetry lines X-Γ-M-R in the irreducible Brillouin zone [see Fig. 1(b)] from 580 K to 14.5 K. Figure 2 visualizes the temperature dependence of $A(\mathbf{k}, \omega)$ at two typical temperatures 580 K and 14.5 K, respectively. In comparison with the available theoretical results by Joseph Wang *et al.*, utilizing a generalized gradient approximation [24], the basic feature of band structures [see Fig. 2(c)] is roughly consistent with each other. For instance, the hole-like orbit around -1 eV at the Γ point and similar hole-like orbit at the M point are generally identical. However, the most striking discrepancy is the narrow quasiparticle $5f$ bands in the vicinity of the Fermi level. It should be pointed out that the enhanced spectral weight of $5f$ states in the Fermi level at low temperature commonly exists in actinide systems [38]. It is speculated that the missing of flat $5f$ bands in the literature [24] is partly ascribed to the underestimation of strong correlation among the $5f$ electrons without fully taking into account the many-body effects.

After inspecting the detailed characteristics of $A(\mathbf{k}, \omega)$ shown in Figs. 2(a) and 2(c), it is identified that only the conduction bands intersect the Fermi level, indicating the mostly localized $5f$ states and incoherent quasiparticle bands at high temperature. With gradual decreasing temperature, the overall band profiles generally remain unchanged except for

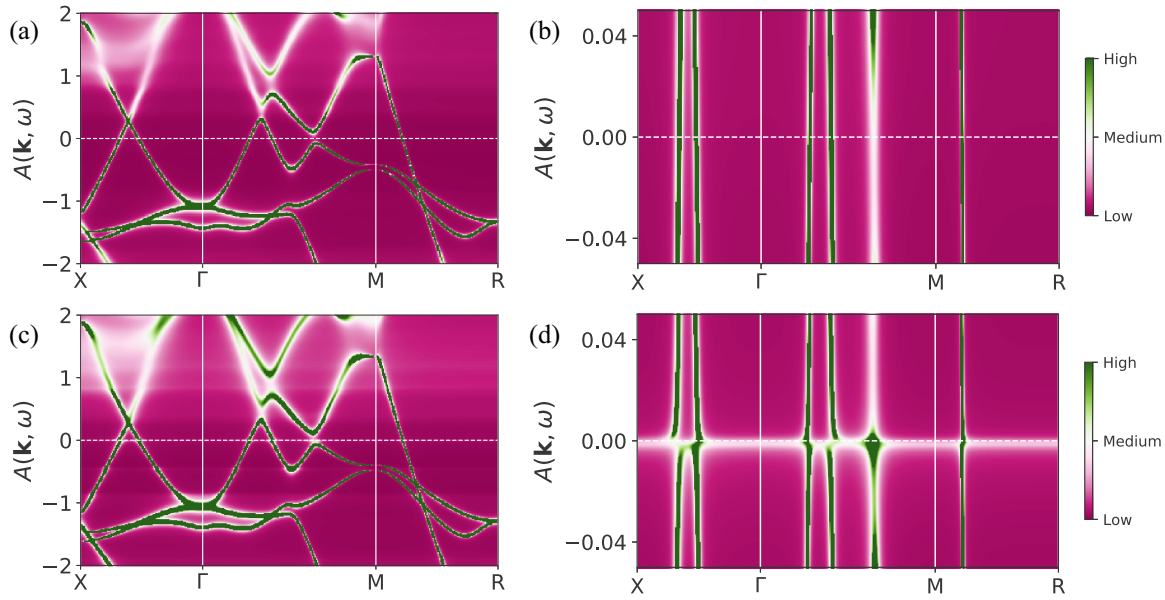

FIG. 2. Momentum-resolved spectral functions $A(\mathbf{k}, \omega)$ of $PuIn_3$ as a function of temperature under ambient pressure obtained by DFT + DMFT calculations. (a) 580 K. (c) 14.5 K. An enlarged view of panel (b) 580 K and (d) 14.5 K in the energy window $\omega \in [-0.05, 0.05]$ eV. In these panels, the horizontal lines denote the Fermi level.

the emergence of flat 5f bands around the Fermi level. In the energy range of -1 eV $\sim$ 1 eV, especially at -0.9 eV and -0.45 eV, there exist nearly dispersionless quasiparticle bands which are associated with 5f states and are split by spin-orbital coupling. At low temperature, 5f states tend to be itinerant and form coherent bands. Along the X-Γ and Γ-M high-symmetry lines, moderate hybridization between 5f bands and 5p valence electrons are observed. It is guessed that the stripe-like patterns, c-f hybridization, and coherent quasiparticle bands possibly reveal a temperature-induced localized to itinerant crossover for 5f states in $PuIn_3$.

B. Density of states

To further explore the electronic structure of $PuIn_3$, we discuss the density of states as a function of temperature in detail. In Fig. 3, we plot the calculated total density of states and experimental photoemission spectroscopy [28] together. Despite the small peaks in our calculated total density of states, the archetypical peaks in experimental photoemission spectroscopy at the Fermi level and -1.2 eV are roughly captured in our calculations. The major difference lies in that the calculated lower Hubbard band is missing in the experimental photoemission spectroscopy. The discrepancies between the theoretical and experimental spectra are likely attributed to the uncertainty in the Coulomb interaction parameters and the use of oversimplified double-counting scheme [35].

Figure 4 shows the electronic density of states at typical temperatures 580 K and 14.5 K. Several features are as follows. First of all, the shapes of total density of states at 580 K and 14.5 K resemble each other despite the quasiparticle peak around the Fermi level at 14.5 K. The spectral weight at the Fermi level is low, which is almost invisible at high temperature. Meanwhile, 5f states are nearly localized to form incoherent states. In addition, the broad "hump" from 0.5 eV to 3 eV is mainly assigned to the upper Hubbard band of 5f orbitals and the lower Hubbard band locates in the energy range of -3 eV and -2 eV. Second, the spectral weights of the upper Hubbard band and lower Hubbard band transfer to the Fermi level as temperature declines. At low temperature, quasiparticle multiplets appear near the Fermi level, manifesting themselves in a pronounced central quasiparticle peak (QP). In addition, there exist two satellite peaks "P1" and "P2" about -0.9 eV and -0.45 eV. The two peaks at high temperature are not as obvious as those at low temperature. Particularly, they are closely linked to the parallel stripe-like traits in momentum-resolved spectral functions $A(\mathbf{k}, \omega)$. It is

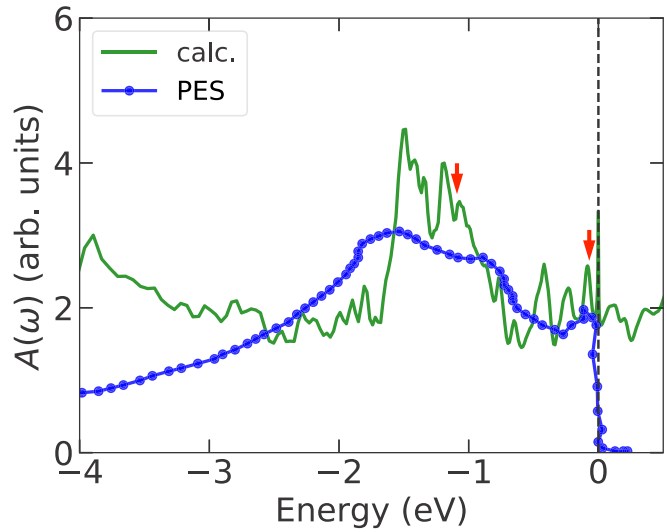

FIG. 3. Electronic density of states of $PuIn_3$. The calculated and experimental data are represented by solid thick line and circles, respectively. The calculated data are multiplied by the Fermi-Dirac distribution function. The experimental data are extracted from Ref. [28] at photon energy of 40.8 eV (blue circles).

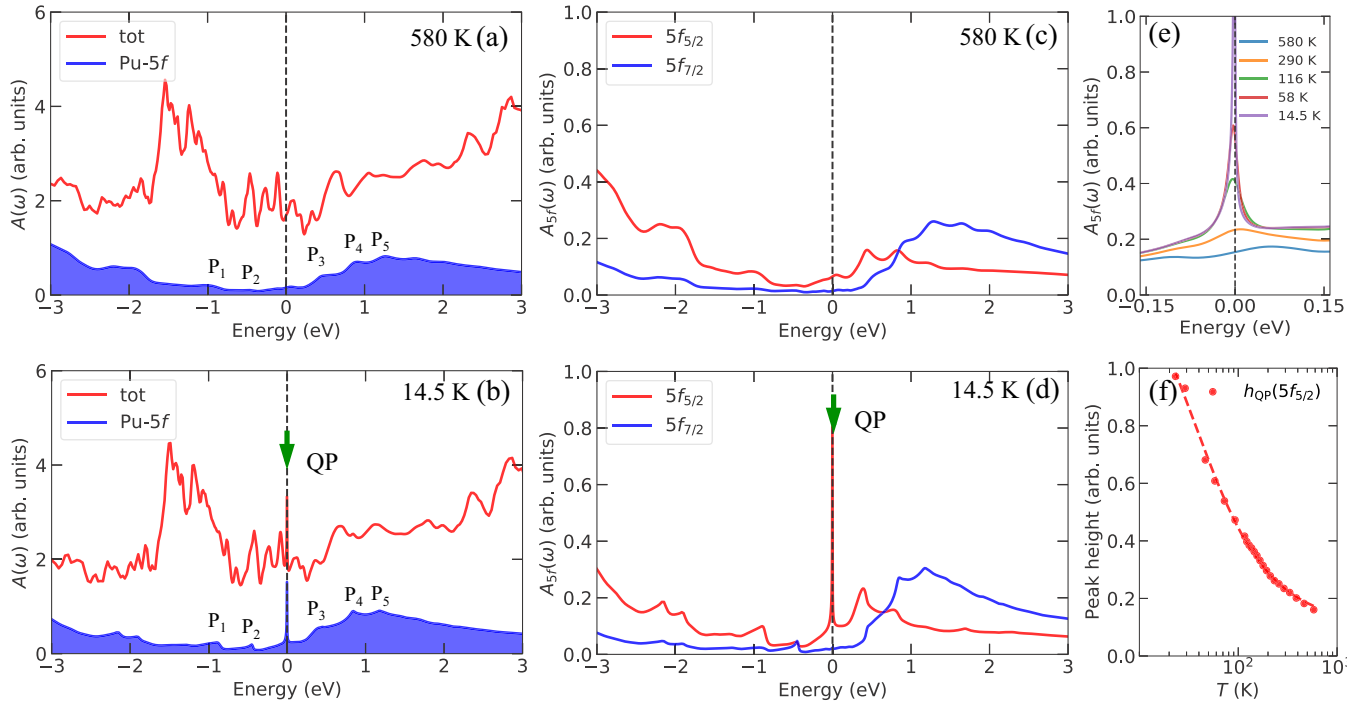

FIG. 4. Electronic density of states of $PuIn_3$. Total density of states (thick solid lines) and partial $5f$ density of states (color-filled regions) of (a) 580 K, (b) 14.5 K. The peaks stemming from the quasiparticle multiplets are annotated with "P1," "P2," "P3," "P4," and "P5". The j-resolved $5f$ partial density of states with $5f_{5/2}$ and $5f_{7/2}$ components represented by red and blue lines, respectively. (c) 580 K, (d) 14.5 K. (e) The evolution of $5f$ density of states against temperature in the vicinity of Fermi level. (f) The height of the central quasiparticle peak $h_{QP}(5f_{5/2})$ as a function of temperature.

known that the central quasiparticle peak together with "P1" and "P2" peaks are similar to the so called "Racah materials" like δ-Pu and PuB_6. It is proposed that these quasiparticle multiplets are in conjunction with the $5f$ valence state fluctuations [39], which may be prominent in some plutonium-based intermetallic compounds. Third, a doublet of reflected peaks above the Fermi level are "P3" and "P4," locating around 0.4 eV and 0.8 eV. Additionally, a small satellite peak "P5" is approximately 1.1 eV. It is noticed that similar quasiparticle multiplets have already been predicted in cubic phase Pu_3Ga [40].

Owing to the spin-orbital coupling [4], the $5f$ orbitals are split into six-fold degenerated $5f_{5/2}$ and eight-fold degenerated $5f_{7/2}$ states. In Fig. 4(d), it is clear that the central quasiparticle peak is mainly constituted by the $5f_{5/2}$ state and a small satellite peak "P2" at -0.45 eV mainly belongs to the $5f_{7/2}$ state, resulting in the energy gap about 0.45 eV. Furthermore, the peak at -1.2 eV is ascribed to the $5f_{5/2}$ state which accords with the experimental photoemission spectroscopy. It is worth mentioning that the $5f_{7/2}$ state remains insulating-like and manifests a gap in the Fermi level. Therefore, the distinguished coherent behavior of the $5f_{5/2}$ state and $5f_{7/2}$ state is orbital selective. Moreover, the "P1" peak is largely from the $5f_{5/2}$ state. While the other satellite peaks ("P3," "P4," and "P5") are built from a mixture of the $5f_{5/2}$ and $5f_{7/2}$ states. Lastly, as is shown in Fig. 4(e), the central quasiparticle peak from $5f_{5/2}$ states becomes sharp and intense at low temperature. The increment of the spectral weight of the central quasiparticle peak with decreasing temperature implies the onset of coherent $5f$ states and appearance of itinerant $5f$ valence electrons. In consequence, it is roughly concluded that a localized to itinerant crossover may occur with a decline of temperature.

C. Fermi surface topology

In this subsection, we examine the Fermi surface topology to unveil the temperature-dependent $5f$ correlated electronic states of $PuIn_3$. The three-dimensional Fermi surface and corresponding two-dimensional Fermi surface at two characteristic temperatures 580 K and 14.5 K are visualized in Fig. 5. It is observed that two doubly degenerated bands intersect the Fermi level (number of bands: 18 and 19, 16 and 17), which are marked by α and β, respectively. The α bands resemble the distorted spherical Fermi surfaces at each of the eight apex angles of the first Brillouin zone, while the β bands located at the Γ point to form an ellipsoid shape. As can be seen, the Fermi surface topology of α and β bands agree quite well with previous theoretical results [24]. Particularly, the β band corroborates the Fermi surface measured by the dHvA experiment [25], demonstrating the accuracy of our calculations. When the temperature goes down, the topology of α bands nearly remains unchanged and the volumes rarely alter either. The key factors lie in the β bands, which experience topology variation and volume expansion. Specifically speaking, the band's intersections with the Fermi level along the Γ-X line [see Figs. 5(c) and 5(f)] enlarges with decreasing temperature, which is in line with the band twist around the Fermi level due to c-f hybridization at low temperature. At high temperature, they cross the Γ-X line to formulate

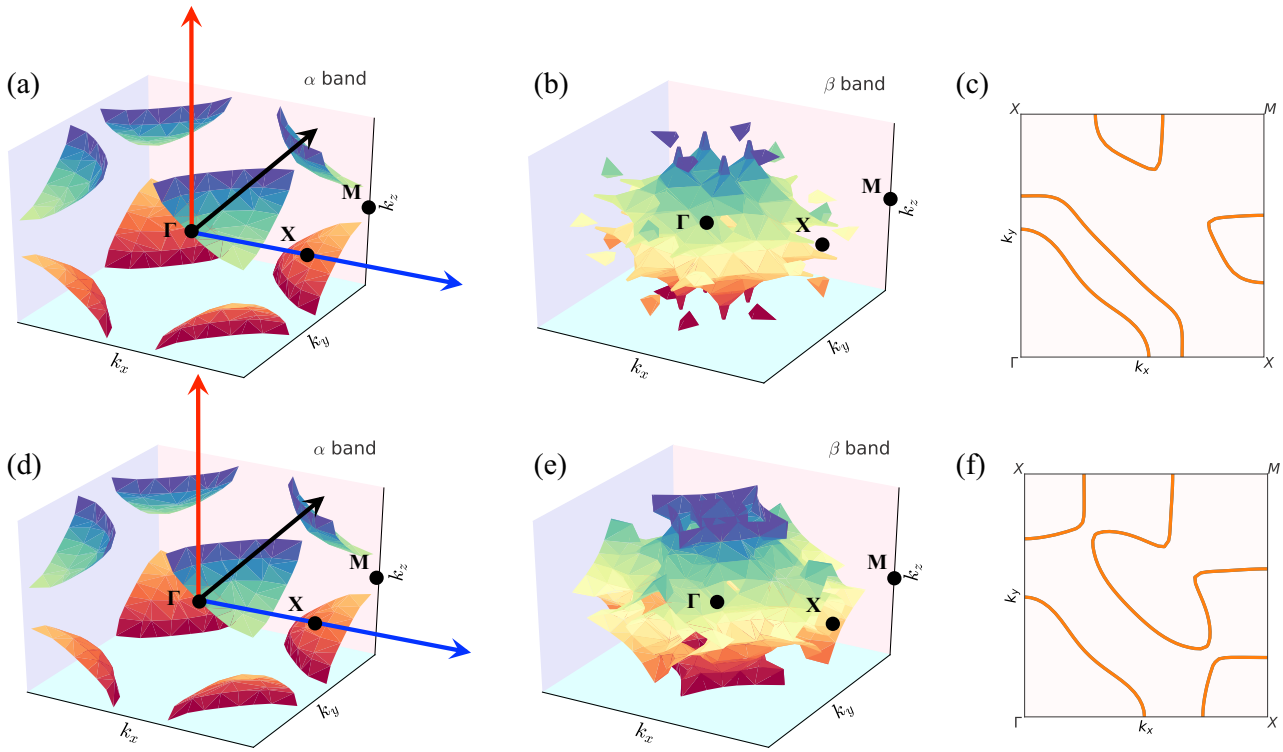

FIG. 5. Three-dimensional Fermi surface and two-dimensional Fermi surface of $PuIn_3$ calculated by the DFT + DMFT method at (a)–(c) 580 K and (d)–(f) 14.5 K. There are two doubly degenerated bands (labelled by α and β) crossing the Fermi level. Three-dimensional Fermi surface of α and β bands are plotted in the left and middle columns, respectively. The right columns denote the two-dimensional Fermi surface on the k_x-k_y plane ($k_z = \pi/2$) corresponding to β bands.

ellipsoid-like Fermi surfaces [see Fig. 5(c)] and they intersect the M-X line at low temperature. So the Fermi surface topologies indeed change tremendously with decreasing temperature, which hints at the possible Lifshitz transition for 5f states and occurrence of low-temperature magnetic order. The transformation of Fermi surface topology is intimately connected with the temperature-driven localized to itinerant crossover of 5f correlated electronic states, which could be detected using quantum oscillation measurements [24].

D. Self-energy functions

As mentioned above, the 5f electrons are strongly correlated and the electronic correlation effects can be deduced from their electron self-energy functions [29,30]. Figure 6 illustrates the renormalized imaginary part of the self-energy functions $Z|\mathrm{Im}\Sigma(\omega)|$ for $5f_{5/2}$ and $5f_{7/2}$ states. Here Z means the quasiparticle weight or renormalization factor, which denotes the electronic correlation strength and can be obtained from the real part of the self-energy functions via the following equation [29]:

$$Z^{-1} = \frac{m^\star}{m_e} = 1 - \frac{\partial \mathrm{Re}\Sigma(\omega)}{\partial \omega}\Big|_{\omega=0}. \quad (1)$$

Generally, $Z|\mathrm{Im}\Sigma(0)|$ is considered as an indicator of low-energy electron scattering rate [41]. At low temperature, $Z|\mathrm{Im}\Sigma_{5f_{5/2}}(0)|$ approaches zero, demonstrating the itinerant nature of 5f states. With elevating temperature, $Z|\mathrm{Im}\Sigma_{5f_{5/2}}(\omega)|$ rises swiftly, especially in the low-energy regime of [−0.5 eV, 0.5 eV], and then reaches finite values. Conversely, $Z|\mathrm{Im}\Sigma_{5f_{7/2}}(\omega)|$ surges up quickly at the high-energy regime ($|\omega| < 0.5$ eV). So the enhancement of $Z|\mathrm{Im}\Sigma_{5f_{7/2}}(\omega)|$ becomes more significant than that of $Z|\mathrm{Im}\Sigma_{5f_{5/2}}(\omega)|$, which leads to the suppression for the itinerancy of the $5f_{7/2}$ state and explains its energy gap in the Fermi

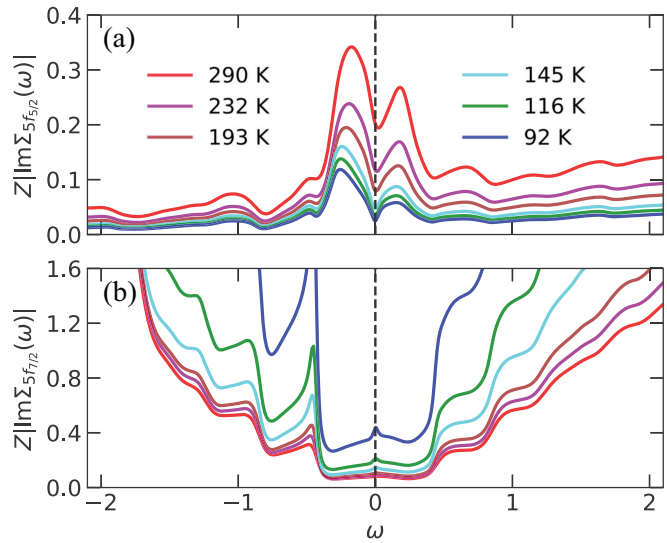

FIG. 6. Renormalized real-frequency self-energy functions of $PuIn_3$ obtained by the DFT + DMFT method. (a) and (b) denote temperature-dependent $Z|\mathrm{Im}\Sigma(\omega)|$ for the $5f_{5/2}$ and $5f_{7/2}$ states, where Z means the renormalization factor.

TABLE I. The electron effective mass $m^\star$ and quasiparticle weight Z of $5f_{5/2}$ and $5f_{7/2}$ states for $PuIn_3$ at temperatures 580 K and 14.5 K, respectively. Here m_e means the bare electron mass.

	$5f_{5/2}$		$5f_{7/2}$	
cases	$m^\star/m_e$	Z	$m^\star/m_e$	Z
580 K	28.60	0.035	3.52	0.28
14.5 K	136.50	0.004	5.25	0.19

level. Since the self-energy functions of the $5f_{5/2}$ and $5f_{7/2}$ states manifest differentiated temperature-dependent patterns, it is concluded that $5f$ electronic correlation are orbital selective.

To explore the band-structure renormalization due to the strong electronic correlations, we obtain the electron effective mass $m^\star$ and quasiparticle weight Z of $5f_{5/2}$ and $5f_{7/2}$ states for $PuIn_3$ from the electronic self-energy functions according to Eq. (1). As Table I lists, the $5f_{7/2}$ component exhibits metallic behavior ($Z \approx 0.28$, $m^\star \approx 3.52m_e$) at 580 K. Even at 14.5 K, the $5f_{7/2}$ component remains a metallic feature with $Z \approx 0.19$, $m^\star \approx 5.25m_e$. However, the $5f_{5/2}$ component is insulating ($Z \approx 0.035$, $m^\star \approx 28.6m_e$) at 580 K and becomes more localized ($Z \approx 0.004$, $m^\star \approx 136.5m_e$) at 14.5 K. Obviously, the electron effective mass of the $5f_{5/2}$ state is much larger than that of the $5f_{7/2}$ state, which indicates a more localized $5f_{5/2}$ state and a stronger electronic correlation [42] at low temperature. In addition, this scenario is regarded as an orbital selective $5f$ insulating state, which is an analogy to the orbital-selective Mott phase identified in the transition metal compounds, such as $Ca_{2-x}Sr_xRuO_4$ [43].

TABLE II. Probabilities of $5f^3$, $5f^4$, $5f^5$, $5f^6$, and $5f^7$ for $PuIn_3$ at temperatures 580 K and 14.5 K, respectively.

Temperatures	$5f^3$	$5f^4$	$5f^5$	$5f^6$	$5f^7$
580 K	1.106×10^{-3}	0.086	0.866	0.047	1.894×10^{-4}
14.5 K	8.917×10^{-4}	0.076	0.862	0.061	2.738×10^{-4}

E. Atomic eigenstate probabilities

In analogy with the archetypal mixed-valence metal δ-Pu [44] whose average $5f$ electron occupation deviated from its nominal value 5.0, $PuIn_3$ is expected to display mixed-valence behavior since it shares some common features like the three-peak structure in the spectral functions of δ-Pu. To interpret the valence-state fluctuations and mixed-valence behavior, we attempt to obtain the $5f$ electron atomic eigenstates from the output of DMFT ground states. Here p_Γ is adopted to quantify the probability of $5f$ electrons which stay in each atomic eigenstate Γ. Then the average $5f$ valence electron is expressed as $\langle n_{5f}\rangle = \sum_\Gamma p_\Gamma n_\Gamma$, where n_Γ is the number of electrons in each atomic eigenstate Γ. Finally, the probability of the $5f^n$ electronic configuration can be defined as $\langle w(5f^n)\rangle = \sum_\Gamma p_\Gamma \delta(n - n_\Gamma)$.

Figures 7(a) to 7(c) depict the calculated probability of $5f^n$ electronic configuration for $PuIn_3$, where $n \in [3, 7]$ and the other probability of electronic configurations are too small to be seen. As listed in Table II, the probability of the $5f^5$ electronic configuration is overwhelmingly dominant, which accounts for 86%, followed by $5f^4$ and $5f^6$ electronic configurations. At 580 K, the probability of $5f^4$ and $5f^6$ electronic configurations stand at 8.6% and 4.7%, respectively. In the meantime, the occupation of the $5f$ electrons is approximately 4.96, which approaches its nominal value 5.0. Hence $5f$ elec-

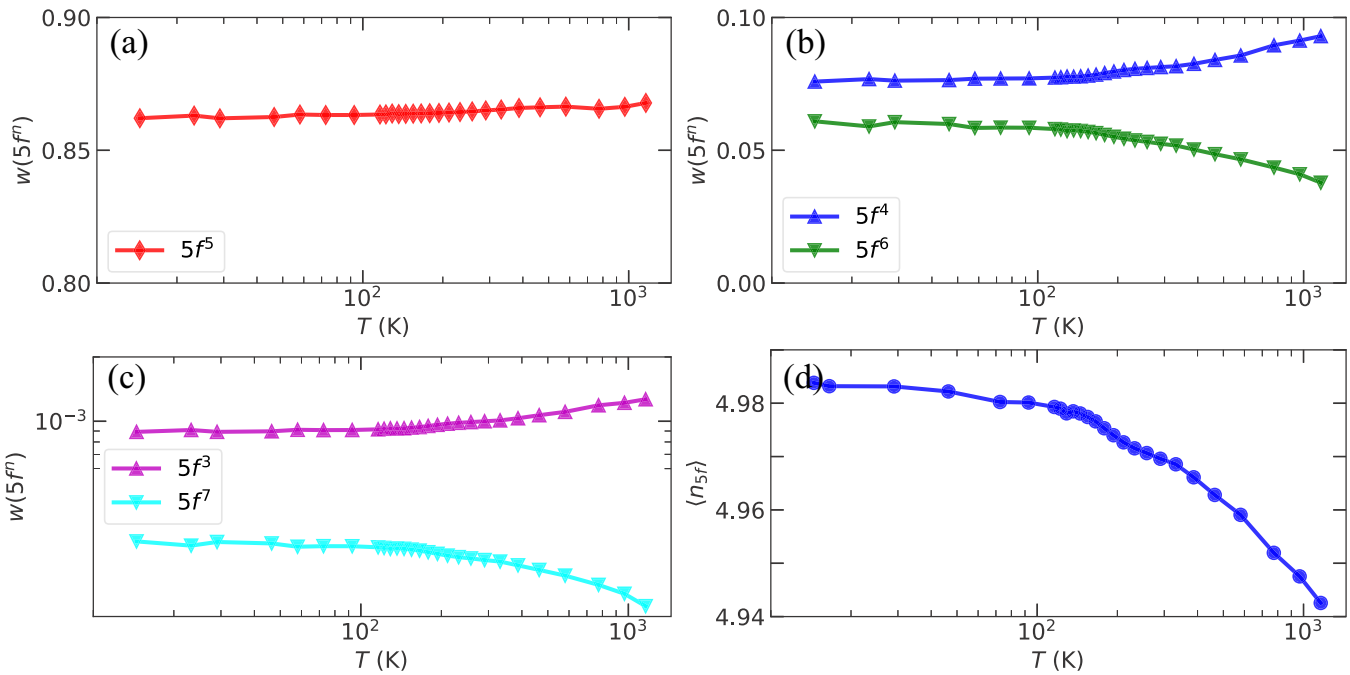

FIG. 7. Probabilities of (a) $5f^5$ (red), (b) $5f^4$ (blue), $5f^6$ (green) configurations, and (c) $5f^3$ (purple), $5f^7$ (cyan), and (d) $5f$ occupancy as a function of temperature for $PuIn_3$ by DFT + DMFT calculations.

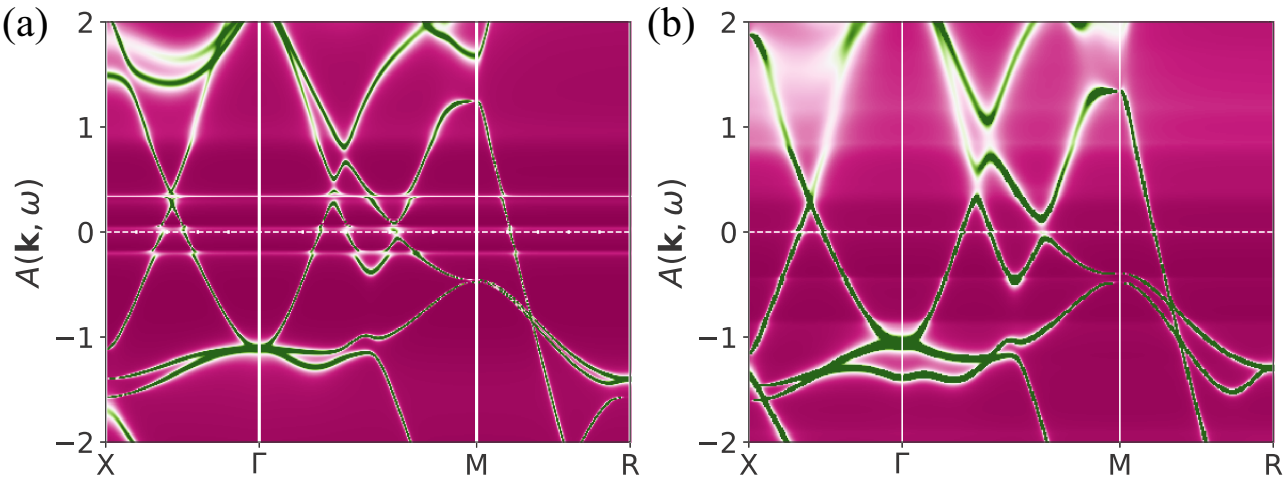

FIG. 8. The momentum-resolved spectral functions $A(\mathbf{k}, \omega)$ of both (a) $CeIn_3$ and (b) $PuIn_3$ along the high-symmetry lines in the Brillouin zone obtained by DFT + DMFT method at 14.5 K. The horizontal dashed lines mean the Fermi level.

trons are inclined to stay more time at the $5f^5$ electronic configuration than the $5f^4$ and $5f^6$ electronic configurations. It means that the valence-state fluctuations are not quite remarkable at relatively high temperature, signifying localized $5f$ states. As the temperature lowers, the probability of the $5f^5$ electronic configuration slightly decreases, accompanied by a subtle deduction of $5f^4$ and a minor growth of $5f^6$ electronic configuration. Overall, the probability of $5f^n$ electronic configurations are not sensitive to varying temperature. As a consequence, the occupation of $5f$ electrons remains almost unchanged, suggesting the atypical mixed-valence behavior of $PuIn_3$, which is beyond our expectation.

IV. DISCUSSION

A. f electrons in $CeIn_3$ and $PuIn_3$

Here we concentrate on the isostructural compounds $CeIn_3$ and $PuIn_3$ to unravel the alluring f electrons and fascinating bonding behavior. As mentioned above, $CeIn_3$ and $PuIn_3$ stabilize in the cubic $AuCu_3$ structure with similar lattice constant 4.689 Å [45] and 4.703 Å [23], respectively. Since the element identification is regarded as the chemical substitution Ce for Pu, the electronic structure and related physical properties are expected to share abundant common traits. For instance, $CeIn_3$ and $PuIn_3$ are typical heavy-fermion compounds [20,46], which develop antiferromagnetic order below Neél temperatures 10 K [47] and 14.5 K [19], respectively.

Figure 8 presents the calculated momentum-resolved spectral functions $A(\mathbf{k}, \omega)$ of both $CeIn_3$ and $PuIn_3$ along the same high-symmetry lines in the Brillouin zone via the DFT + DMFT method at 14.5 K. Several features are as follows. First, the parallel flat bands at 0.1 eV and 0.4 eV [see Fig. 8(a)] are attributed to Ce-$4f$ electrons, which are split by spin-orbital coupling into $j = 5/2$ and $j = 7/2$ subbands with energy separation being approximately 0.3 eV. Second, the narrow $4f$ bands intersect conduction bands to form c-f hybridization. Third, the electron-like band and hole-like band only adjoin along the X-Γ line in the angle-resolved photoemission spectroscopy experiment [48], which is well reproduced by our calculation. Fourth, the conduction bands with strong energy dispersions are mainly contributed by In atoms. Consequently, the electron-like band and hole-like band at Γ and M points located about −1 eV and −0.5 eV below the Fermi level, respectively.

For comparison, it is significative to evaluate the band structure of $PuIn_3$ [see Fig. 8(b)]. First of all, the overall energy profiles seem incredibly similar for $CeIn_3$ and $PuIn_3$, even though the band degeneracy at the Γ point in $CeIn_3$ is lifted in $PuIn_3$. Such amazing similarity in the band structure is attributed to the conduction band of In atoms. Second, the dispersionless flat $5f$ bands mainly distribute at −0.9 eV and −0.45 eV below the Fermi level, where the spin-orbital coupling energy separation between $j = 5/2$ and $j = 7/2$ states of $5f$ electrons is about 0.45 eV. It is reasonable that the stronger spin-orbital coupling strength of Pu results in a larger energy separation than that of Ce because the atomic number of Pu is much higher than that of Ce. Third, both $4f$ and $5f$ states are strongly correlated with strikingly renormalized bands and electron effective masses.

To further discuss the itinerant degree of f electrons, density of states, hybridization functions, and the probability of atomic eigenstates are analyzed. As is shown in Fig. 9, remarkable quasiparticle multiplets emerge around the Fermi level for $CeIn_3$ and $PuIn_3$, indicating the itinerant f states at low temperature. Since the hybridization functions encapsulate the bonding behavior of f electrons, the finite hybridization functions around the Fermi level of both $CeIn_3$ and $PuIn_3$ manifest f hybridization with conduction bands and the f states grow partially itinerant at low temperature. In addition, the hybridization functions about the Fermi level seem a bit obvious in $PuIn_3$ than those of $CeIn_3$. Now that the density of states and hybridization functions qualitatively depict the itinerant degree of f states, the probability of atomic eigenstate quantifies the hybridization strength and itinerancy of f electrons. As mentioned above, the probability of the $5f^5$ electronic configuration is dominant, followed by $5f^4$ and $5f^6$ electronic configurations. While the leading $4f^1$ electronic configuration with probability about 94% experiences less valence-state fluctuations. Thus the valence-state

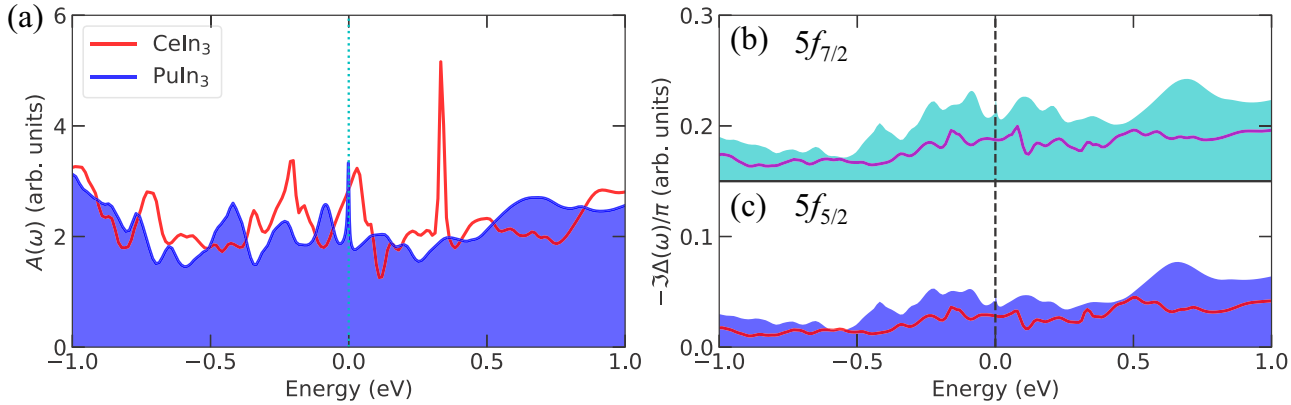

FIG. 9. Total density of states and hybridization functions of $CeIn_3$ and $PuIn_3$ obtained by DFT + DMFT method at 14.5 K. (a) Total density of states of $CeIn_3$ (red) and $PuIn_3$ (blue-filled region). (b) Hybridization functions of $5f_{7/2}$ states for $CeIn_3$ (purple line) and $PuIn_3$ (cyan-filled region). (c) Hybridization functions of $5f_{5/2}$ states for $CeIn_3$ (red line) and $PuIn_3$ (blue-filled region).

fluctuations are not quite remarkable for $CeIn_3$ and $PuIn_3$ at low temperature, which suggest moderate hybridization and partial itinerancy of f electrons.

B. dHvA quantum oscillation

dHvA quantum oscillation is known as a useful tool to detect the Fermi surface. The dHvA effect encodes the magnetic field dependence of the quantum oscillations in magnetization and other properties owing to the change in the occupation of Landau levels driven by the oscillation of the magnetic field. An oscillation frequency proportional to the extremal Fermi surface cross-sectional area perpendicular to the magnetic field direction is expressed as

$$F = \frac{\hbar}{2\pi e} A, \tag{2}$$

where F is the dHvA frequency in units of kT, e is the elementary charge, $\hbar$ is the reduced Planck constant, and A denotes the extremal area. Moreover, the electron effective mass averaged around the extremal orbits can be obtained from the damping strength as a function of temperature. Thus the dHvA frequency and electron effective mass are evaluated using the numerical algorithm implemented by Rourke and Julian [49]. In comparison with dHvA experimental results, the magnetic field is chosen along the [111] direction. The calculated dHvA frequency together with electron effective mass are listed in Table III. The calculated dHvA frequency of the β band is 1.91 kT, which is close to the experimental value about 2.0 kT and theoretical value 2.18 kT [25] based on the $5f$-itinerant band model. However, our calculated dHvA frequency differs from the value using a generalized gradient approximation [24]. These discrepancies might arise from the approximations of DFT calculation methods. Furthermore, the obtained electron effective mass is 1.45 m_e, approaching the previous theoretical value 1.56 m_e [25]. In view of the accordance between the theoretical and experimental results, it is guessed that the electronic correlations [50] indeed affects the Fermi surface and electron effective mass because the discrepancy exists between DFT results and experimental dHvA frequencies for the paramagnetic state of $PuIn_3$. Additionally, the other orbits are not discussed here, which might serve as a critical prediction for further dHvA experiments.

TABLE III. The calculated dHvA frequency and electron effective mass of $PuIn_3$ with magnetic field along the [111] direction. h means hole-like orbit, e denotes electron-like orbit.

F (kT)	$m^*(m_e)$	Type
1.91	1.45	e
5.33	4.62	e
7.68	6.57	e
9.10	7.39	h

As we discussed in Sec. III D, it is discovered that the electron effective mass is indeed significantly enhanced at 14.5 K compared to that at 580 K. While the cyclotron mass listed in Table III gives another way to characterize the electron mass. It is found that the cyclotron mass exhibits a slight mass enhancement compared to the free electron. Being different from the cyclotron mass, the electron effective mass derived from electronic self-energy functions according to Eq. (1) is listed in Table I. It is worth mentioning that Eq. (1) is an approximate form to describe the electron mass and it is temperature dependent. So the absolute value may not be an accurate description of electron effective mass. Only the relative values of the electron effective mass at different temperatures could quantify the electronic correlation strength. The electron effective mass is immensely renormalized at low temperature, implying a stronger electronic correlation as well.

V. CONCLUSION

In summary, we studied the detail electronic structures of $PuIn_3$ by employing a state-of-the-art first-principles many-body approach. The temperature dependence of itinerant to localized crossover and the correlated electronic states were addressed systematically. The $5f$ states retain a strongly correlated nature both at high temperature and low temperature, and the overall system remains metallic. As the

temperature declines, the augmented itinerancy of 5f electrons with significant c-f hybridization and the emergence of valence-state fluctuations indicate a localized-itinerant crossover. Specifically, 5f states manifest orbital-selective electronic correlation, reflected by orbital-dependent electron effective masses and renormalized bands. Our results not only provide a comprehensive picture about the evolution of 5f correlated electronic states with respect to temperature, but also gain important implications into the low-temperature magnetism in $PuIn_3$. Further studies about the other Pu-based compounds are undertaken.

ACKNOWLEDGMENTS

This work was supported by the National Natural Science Foundation of China (Grants No. 11704347, No. 11874329, No. 11934020, and No. 22025602) and the Science Challenge Project of China (Grant No. TZ2016004).

[1] H. G. Smith, N. Wakabayashi, W. P. Crummett, R. M. Nicklow, G. H. Lander, and E. S. Fisher, Phys. Rev. Lett. **44**, 1612 (1980).
[2] J. L. Smith and R. G. Haire, Science **200**, 535 (1978).
[3] N. G. Cooper, Los Alamos Science **26**, 1 (2000).
[4] K. T. Moore and G. van der Laan, Rev. Mod. Phys. **81**, 235 (2009).
[5] R. C. Albers, Nature (London) **410**, 759 (2001).
[6] S. S. Hecker, Metall. Mater. Trans. A **35**, 2207 (2004).
[7] J. C. Lashley, A. Lawson, R. J. McQueeney, and G. H. Lander, Phys. Rev. B **72**, 054416 (2005).
[8] M. Janoschek, P. Das, B. Chakrabarti, D. L. Abernathy, M. D. Lumsden, J. M. Lawrence, J. D. Thompson, G. H. Lander, J. N. Mitchell, S. Richmond, M. Ramos, F. Trouw, J.-X. Zhu, K. Haule, G. Kotliar, and E. D. Bauer, Sci. Adv. **1**, 1500188 (2015).
[9] N. Lanatà, Y. Yao, C.-Z. Wang, K.-M. Ho, and G. Kotliar, Phys. Rev. X **5**, 011008 (2015).
[10] X. Dai, S. Y. Savrasov, G. Kotliar, A. Migliori, H. Ledbetter, and E. Abrahams, Science **300**, 953 (2003).
[11] J. Wong, M. Krisch, D. L. Farber, F. Occelli, A. J. Schwartz, T.-C. Chiang, M. Wall, C. Boro, and R. Xu, Science **301**, 1078 (2003).
[12] T. Das, J.-X. Zhu, and M. J. Graf, Phys. Rev. Lett. **108**, 017001 (2012).
[13] J. J. Joyce, J. M. Wills, T. Durakiewicz, M. T. Butterfield, E. Guziewicz, J. L. Sarrao, L. A. Morales, A. J. Arko, and O. Eriksson, Phys. Rev. Lett. **91**, 176401 (2003).
[14] J. L. Sarrao, L. A. Morales, J. D. Thompson, B. L. Scott, G. R. Stewart, F. Wastin, J. Rebizant, P. Boulet, E. Colineau, and G. H. Lander, Nature (London) **420**, 297 (2002).
[15] N. J. Curro, T. Caldwell, E. D. Bauer, L. A. Morales, M. J. Graf, Y. Bang, A. V. Balatsky, J. D. Thompson, and J. L. Sarrao, Nature (London) **434**, 622 (2005).
[16] D. Daghero, M. Tortello, G. A. Ummarino, J. C. Griveau, E. Colineau, R. Eloirdi, A. B. Shick, J. Kolorenc, A. I. Lichtenstein, and R. Caciuffo, Nat. Commun. **3**, 786 (2012).
[17] X. Deng, K. Haule, and G. Kotliar, Phys. Rev. Lett. **111**, 176404 (2013).
[18] A. P. Dioguardi, H. Yasuoka, S. M. Thomas, H. Sakai, S. K. Cary, S. A. Kozimor, T. E. Albrecht-Schmitt, H. C. Choi, J.-X. Zhu, J. D. Thompson, E. D. Bauer, and F. Ronning, Phys. Rev. B **99**, 035104 (2019).
[19] H. Chudo, G. Koutroulakis, H. Yasuoka, E. D. Bauer, P. H. Tobash, J. N. Mitchell, and J. D. Thompson, J. Phys.: Condens. Matter **26**, 036001 (2013).
[20] E. D. Bauer and J. D. Thompson, Annu. Rev. Condens. Matter Phys. **6**, 137 (2015).
[21] E. D. Bauer, J. D. Thompson, J. L. Sarrao, L. A. Morales, F. Wastin, J. Rebizant, J. C. Griveau, P. Javorsky, P. Boulet, E. Colineau, G. H. Lander, and G. R. Stewart, Phys. Rev. Lett. **93**, 147005 (2004).
[22] A. B. Shick, V. Janiš, and P. M. Oppeneer, Phys. Rev. Lett. **94**, 016401 (2005).
[23] E. D. Bauer, P. H. Tobash, J. N. Mitchell, and J. L. Sarrao, Philos. Mag. **92**, 2466 (2012).
[24] C.-C. Joseph Wang, M. D. Jones, and J.-X. Zhu, Phys. Rev. B **88**, 125106 (2013).
[25] Y. Haga, D. Aoki, H. Yamagami, T. D. Matsuda, K. Nakajima, Y. Arai, E. Yamamoto, A. Nakamura, Y. Homma, Y. Shiokawa, and Y. Ōnuki, J. Phys. Soc. Jpn. **74**, 2889 (2005).
[26] Y. Haga, D. Aoki, H. Yamagami, T. Matsuda, K. Nakajima, Y. Arai, E. Yamamoto, A. Nakamura, Y. Homma, Y. Shiokawa, and Y. Ōnuki, J. Alloys Compd. **444**, 114 (2007).
[27] Y. Haga, E. D. Bauer, P. H. Tobash, J. N. Mitchell, and Z. Fisk, J. Korean Phys. Soc. **63**, 380 (2013).
[28] J. Joyce, J. Wills, T. Durakiewicz, M. Butterfield, E. Guziewicz, D. Moore, J. Sarrao, L. Morales, A. Arko, O. Eriksson, A. Delin, and K. Graham, Phys. B **378**, 920 (2006).
[29] A. Georges, G. Kotliar, W. Krauth, and M. J. Rozenberg, Rev. Mod. Phys. **68**, 13 (1996).
[30] G. Kotliar, S. Y. Savrasov, K. Haule, V. S. Oudovenko, O. Parcollet, and C. A. Marianetti, Rev. Mod. Phys. **78**, 865 (2006).
[31] P. Blaha, K. Schwarz, G. Madsen, D. Kvasnicka, and J. Luitz, *WIEN2k, An Augmented Plane Wave + Local Orbitals Program for Calculating Crystal Properties* (Karlheinz Schwarz, Techn. Universität Wien, Austria, 2001).
[32] K. Haule, C.-H. Yee, and K. Kim, Phys. Rev. B **81**, 195107 (2010).
[33] J. P. Perdew, K. Burke, and M. Ernzerhof, Phys. Rev. Lett. **77**, 3865 (1996).
[34] T. Fujiwara and M. Korotin, Phys. Rev. B **59**, 9903 (1999).
[35] V. I. Anisimov, F. Aryasetiawan, and A. I. Lichtenstein, J. Phys.: Condens. Matter **9**, 767 (1997).
[36] K. Stahrenberg, T. Herrmann, K. Wilmers, N. Esser, W. Richter, and M. J. G. Lee, Phys. Rev. B **64**, 115111 (2001).
[37] K. Haule, Phys. Rev. B **75**, 155113 (2007).
[38] L. Huang and H. Lu, Phys. Rev. B **101**, 125123 (2020).
[39] C.-H. Yee, G. Kotliar, and K. Haule, Phys. Rev. B **81**, 035105 (2010).
[40] L. Huang and H. Lu, arxiv:2102.02034.
[41] W. H. Brito and G. Kotliar, Phys. Rev. B **99**, 125113 (2019).
[42] G. Zwicknagl, Rep. Prog. Phys. **79**, 124501 (2016).

[43] V. Anisimov, I. Nekrasov, D. Kondakov, T. Rice, and M. Sigrist, Euro. Phys. J. B **25**, 191 (2002).

[44] J. H. Shim, K. Haule, and G. Kotliar, Nature (London) **446**, 513 (2007).

[45] A. Benoit, J. X. Boucherle, P. Convert, J. Flouquet, J. Palleau, and J. Schweizer, Solid State Commun. **34**, 293 (1980).

[46] G. Knebel, D. Braithwaite, P. C. Canfield, G. Lapertot, and J. Flouquet, Phys. Rev. B **65**, 024425 (2001).

[47] J. M. Lawrence and S. M. Shapiro, Phys. Rev. B **22**, 4379 (1980).

[48] Y. Zhang, H. Lu, X. Zhu, S. Tan, Q. Liu, Q. Chen, W. Feng, D. Xie, L. Luo, Y. Liu, H. Song, Z. Zhang, and X. Lai, Sci. Rep. **6**, 33613 (2016).

[49] P. Rourke and S. Julian, Comput. Phys. Commun. **183**, 324 (2012).

[50] R. M. Tutchton, W.-t. Chiu, R. C. Albers, G. Kotliar, and J.-X. Zhu, Phys. Rev. B **101**, 245156 (2020).